Spin Hall Effects in Metallic Antiferromagnets

Wei Zhang, Matthias B. Jungfleisch, Wanjun Jiang, John E. Pearson, and Axel Hoffmann

Materials Science Division, Argonne National Laboratory, Argonne, Illinois 60439, USA

Frank Freimuth and Yuriy Mokrousov

Peter Grünberg Institut and Institute for Advanced Simulation, Forschungszentrum Jülich and JARA, D-52425 Jülich, Germany

We investigate four CuAu-I-type metallic antiferromagnets for their potential as spin current detectors using spin pumping and inverse spin Hall effect. Nontrivial spin Hall effects were observed for FeMn, PdMn, and IrMn while a much higher effect was obtained for PtMn. Using thickness-dependent measurements, we determined the spin diffusion lengths of these materials to be short, on the order of 1 nm. The estimated spin Hall angles of the four materials follow the relationship PtMn > IrMn > PdMn > FeMn, highlighting the correlation between the spin-orbit coupling of nonmagnetic species and the magnitude of the spin Hall effect in their antiferromagnetic alloys. These experiments are compared with first-principles calculations. Engineering the properties of the antiferromagnets as well as their interfaces can pave the way for manipulation of the spin dependent transport properties in antiferromagnet-based spintronics.

The detection of pure spin currents via the inverse spin Hall effect (ISHE) [1–3] is a promising route towards energy-efficient spintronics [4]. Towards this end, the discovery of new spin-detector materials has focused on normal metals (NMs), such as Pt, Ta, and W [5–7]. The intense interest in spin current detection requires understanding of ISHE in materials beyond NMs. Recently, spin-detector materials have been extended to ferromagnets (FM) such as permalloy (Py) with comparable efficiency to Pt [8]. However, additional FM ordering and other confounding effects of anisotropic magnetoresistance (AMR) limit the possible applications in dynamic experiments [9]. In contrast, antiferromagnets (AF) with exotic properties (e.g., zero net magnetization, nontrivial spin-orbit coupling, and nonlinear magnetism) have attracted increasing attention [10–14] and are promising for higher-frequency applications beyond ferromagnetic resonance. A large anomalous Hall effect and spin Hall effect (SHE) have been theoretically proposed in γ-FeMn, IrMn$_3$ and Cr, owing to the large spin-orbit coupling of heavy atoms and the Berry phase of the noncollinear spin textures [15–17]. These pioneering theoretical works emphasize the need for searching new efficient AF spin current detectors material-wise as well as experiments investigating the role of heavy elements for the spin-orbit properties of their AF alloys. In this context, important spin-transport parameters need to be determined, which include the spin Hall angle (γ_{SH}), spin diffusion length (λ_{sf}), and/or spin dephasing length [18,19], as well as the influence from interface characteristics such as spin mixing conductance (g_{mix}), spin-memory loss, and exchange interactions [20–23].

In this work, we present measurements of four different CuAu-I-type AFs with the same chemical structure, i.e.,

$X_{50}Mn_{50}$ where $X = $ Fe, Pd, Ir, and Pt (with increasing atomic number) as spin current detector materials. The CuAu-I-type AFs are of significant interest due to their simple structure as well as the possibility of epitaxial growth on many FMs, which are crucial for many spintronics applications. Spin pumping and ISHE experiments were carried out on Py(15)/AF(t) bilayer and Py(15)/Cu(4)/AF(t) multilayer structures (all thicknesses, including t, are in nm). The Cu(4) layer breaks the FM/AF magnetic exchange coupling, yet it does not alter the spin propagation between the FM and AF due to the fact that the spin diffusion length of Cu is much longer than 4 nm at room temperature (RT) (Fig. 1). We fabricated the devices using magnetron sputtering and photolithography [24]. The bilayers and multilayers were prepared in the shape of a 20 μm $\times$ 2 mm stripe using lithography and lift-off on intrinsic Si substrates with 300-nm thick thermally grown SiO$_2$. The electrical leads and the coplanar waveguide (CPW) were subsequently fabricated on top of the bilayers or trilayers. An 80-nm-thick MgO spacer was used to separate the multilayer stack from the CPW. The resistivity values of the AFs were characterized independently using a four-probe method, yielding 167.7 $\mu\Omega$cm for FeMn, 223.0 $\mu\Omega$cm for PdMn, 269.3 $\mu\Omega$cm for IrMn, and 164.0 $\mu\Omega$cm for PtMn, respectively. For the spin pumping measurements, the frequency was kept between 4 and 9 GHz and the rf power was 10 dBm.

Figure 2 illustrates the dc voltages (V_{dc}) measured at 9 GHz for the four different AF materials in the Py/Cu/AF (5) structure. The signals have superimposed symmetric and antisymmetric Lorentzian components. The antisymmetric component is attributed to the homodyne AMR while the symmetric component results from the ISHE
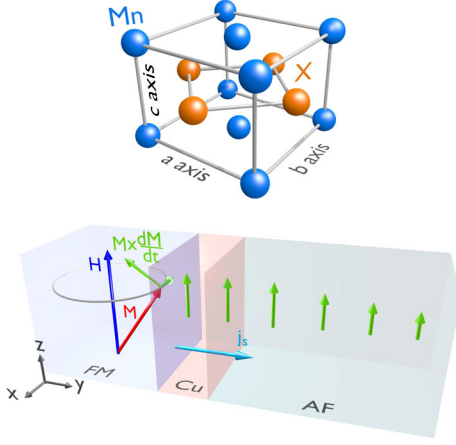
FIG. 1 (color online). A sketch illustrating the chemical structure of CuAu-I-type AFs (X = Fe, Pd, Ir, Pt) and the spin pumping and spin Hall effect experiment for the Py/Cu/AF structures.

FIG. 2 (color online). AMR-ISHE spectra measured at 9 GHz of the Py(15)/Cu(4)/AF(5) structure for FeMn, PdMn, IrMn, and PtMn at RT.

[25,26]. The positive polarity of the ISHE voltage with respect to the AMR indicates a positive spin Hall angle for all four materials. Since both the ISHE and AMR components have the same power dependence, the resultant dc voltage is a sum of the two [25,26]. We define a parameter W_{ISHE}, which represents the weight of the symmetric component (ISHE). W_{ISHE} can be further expressed in the form of $W_{\text{ISHE}} = 1/(1 + V_{\text{AMR}}/V_{\text{ISHE}})$, and the ratio of the two components can be written as [27]

$$\frac{V_{\text{ISHE}}}{V_{\text{AMR}}} = \frac{\gamma_{\text{SH}} e L E f g_{\text{mix}} \lambda_{\text{sf}}}{R_{\text{CPW}} I_{\text{CPW}} \frac{\Delta R_{\text{FM}}}{R_{\text{FM}}}} \frac{h_{\text{rf}}}{\Delta H} \frac{\rho_{\text{FM}}}{t_{\text{FM}}} \tanh\left(\frac{t_{\text{AF}}}{2\lambda_{\text{sf}}}\right), \quad (1)$$

where γ_{SH} is the spin Hall angle, L is the device length, E is the ellipticity correction, R_{CPW} is the CPW resistance, I_{CPW} is the microwave current passing along the CPW, $\Delta R_{\text{FM}}/R_{\text{FM}}$ is the FM anisotropic magnetoresistance, h_{rf} is the Oersted field, ΔH is the linewidth, and ρ_{FM} is the FM resistivity [27]. Notably, the AF thickness dependence is only contained in the distribution of the spin accumulation $\tanh(t_{\text{AF}}/2\lambda_{\text{sf}})$. Therefore, the spin diffusion length can be extracted from fitting the thickness-dependent ratio W_{ISHE} (Fig. 3). This model was initially used for Py/NM bilayers, but it can be applied to the current scenario due to the facts that (1) Cu has a negligible spin Hall effect and long spin diffusion length (on the order of hundreds of nm), and (2) Cu shunts the voltages from both AMR and ISHE; therefore, the parameter W_{ISHE} is weakly affected. Experimentally, we found that the absolute values of W_{ISHE} for Py/AF are almost the same as with Py/Cu/AF but only slightly smaller, and the thickness dependence of W_{ISHE} is almost identical for the two sets of samples. One possible explanation of the smaller W_{ISHE} values for Py/AF could be the exchange spring effect [28,29] causing an additional AMR contribution from the AF moments oscillating together with the Py moments [10,13]. We obtain the spin
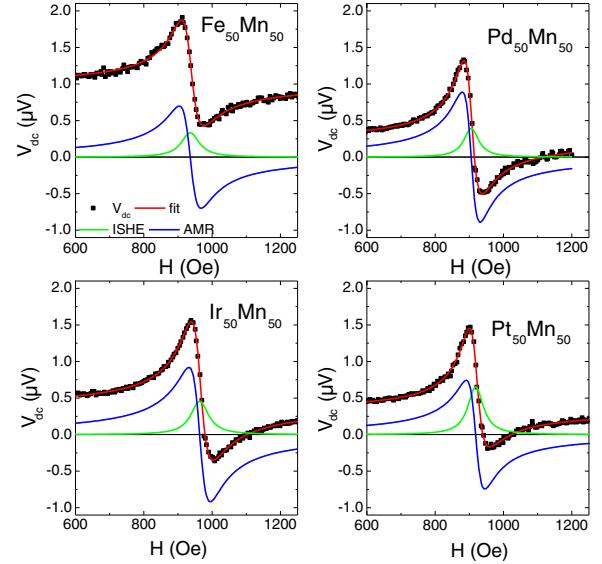
diffusion lengths for the four AF materials (Fig. 3): $\lambda_{\text{sf(FeMn)}} = 1.8 \pm 0.5$ nm, $\lambda_{\text{sf(PdMn)}} = 1.3 \pm 0.1$ nm, $\lambda_{\text{sf(IrMn)}} = 0.7 \pm 0.2$ nm, and $\lambda_{\text{sf(PtMn)}} = 0.5 \pm 0.1$ nm. Such small spin diffusion lengths are comparable to the mean free paths estimated from their resistivity values; however, the diffusion model, which lays the foundation of the above analysis, is still valid in this limit [30].

In Eq. (1), only the spin Hall angle γ_{SH}, spin mixing conductance g_{mix}, and spin diffusion length λ_{sf} are specific parameters related to the AF materials (spin current detector). Therefore, W_{ISHE} can be rewritten as

$$W_{\text{ISHE}} = \left(1 + \frac{1}{C\gamma_{\text{SH}} g_{\text{mix}} \lambda_{\text{sf}} \tanh\left(\frac{t_{\text{AF}}}{2\lambda_{\text{sf}}}\right)}\right)^{-1}, \quad (2)$$

where C depends on f and is otherwise only a function of the CPW and FM layer, and is thus independent of the AFs. We note that for very thin AF layers, it is likely that the Néel temperatures may be below RT due to the finite size effects [31,32], which may affect the determination of λ_{sf}. Using a phenomenological model [31] and realistic parameters [33] we estimate the critical thicknesses for paramagnetic to antiferromagnetic transitions at RT to be ~1–2 nm for all the AFs studied here. However, at sufficiently high AF thickness, t_{AF} ($> 3\lambda_{\text{sf}}$), the AF layers are antiferromagnetically ordered and the W_{ISHE} also saturates with the AF thickness [$\tanh(t_{\text{AF}}/2\lambda_{\text{sf}}) \approx 1$], i.e., $W_{\text{ISHE}}^{\text{sat}} = [1 + (1/C\gamma_{\text{SH}} g_{\text{mix}} \lambda_{\text{sf}})]^{-1}$. We use the $W_{\text{ISHE}}^{\text{sat}}$ values obtained from the thicker samples ($t_{\text{AF}} \geq 5$ nm) for the determination of γ_{SH} of the antiferromagnetically ordered phases. According to Fig. 3, $W_{\text{ISHE}}^{\text{sat}}$ values of the four AFs at 9 GHz are 0.22 ± 0.01 (FeMn), 0.18 ± 0.01 (PdMn), 0.18 ± 0.01 (IrMn), and 0.31 ± 0.01 (PtMn). Using the λ_{sf} values determined above and neglecting the variation of
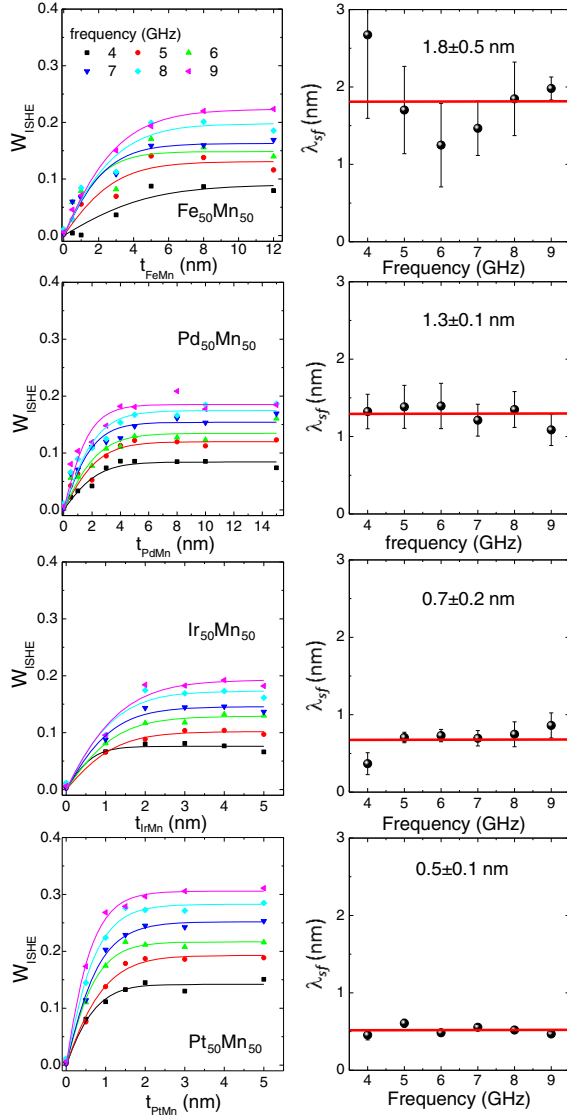
FIG. 3 (color online). Thickness dependence of the weight W_{ISHE} of the symmetric component and estimation of the spin diffusion length for FeMn, PdMn, IrMn, and PtMn at RT.

g_{mix} for now, we estimated the relative strength of the spin Hall angle (using FeMn as reference) of the four AF materials, FeMn:PdMn:IrMn:PtMn = 1:1.1:2.1:5.7. This result is not unexpected, since recent theoretical work [16] attributed the origin of the anomalous Hall effect of IrMn$_3$ not only to the triangular spin textures but also to the large spin orbit coupling of the heavy Ir atoms which is transferred to the magnetic Mn atoms by their hybridization. Further, another experiment showed that the spin-orbit strength of a nonmagnetic metal in a magnetic alloy directly dictates the magnitude of the anomalous Hall effect [34]. Therefore the 5d-metal-alloy AFs (PtMn and IrMn) are expected to exhibit stronger intrinsic SHE than the 4d-metal-alloy PdMn, which is further stronger than the 3d-metal-alloy FeMn. Recent work has demonstrated quantitative scaling of the spin Hall angle with the atomic

number in a series of noble metals [35]. Our results further highlight the important role of the spin-orbit coupling of the heavy elements for the properties of their simple alloys which also acquire a sizable spin-orbit effect due to the transfer of spin-orbit coupling through their orbital hybridization [16,34].

In order to determine the spin Hall angle and spin Hall conductivity quantitatively from the experimental data, it is also necessary to determine the spin mixing conductance g_{mix}, which is usually extracted from the damping enhancement ($\Delta\alpha$) in the spin pumping experiment. For paramagnetic metals, the damping enhancement is mostly related to bulk spin absorption. However, additional contribution may arise due to magnetic ordering of interfaces [19,36]. For Py/Cu/AF structures, it has been found that the spin mixing and the spin-to-charge conversion are driven by the Cu/AF interface and the AF spin absorption, respectively [18,22,23]. For Py/AF structures, the spin mixing is affected by interface magnetic ordering and exchange coupling.

We present data for IrMn as an example. As illustrated in Fig. 4, the linewidth for Py/IrMn is higher than that for Py/Cu/IrMn, and both are greater than for pure Py. The damping enhancement can thus be extracted from a linear fit for the frequency dependence of the linewidth broadening (ΔH) [25,27]. As shown in Fig. 4(a), the damping enhancement for Py/Cu/IrMn is around $\Delta\alpha = 1 \times 10^{-3}$. g_{mix} is estimated around $12\,\mathrm{nm}^{-2}$ via $g_{mix} = (4\pi M_s t_{FM}/g\mu_B)\Delta\alpha$ [21,25,27], where g, μ_B, and M_s are the Landé g factor, Bohr magneton, and saturation magnetization of Py, respectively. Measurements on FeMn, PdMn, and PtMn show less discernable damping enhancement. In order to compare our measurements to the theoretical calculations, we assume the same value of g_{mix} for all measured AFs. Using the predetermined resistivity values of each AF, we estimated the spin Hall angle of the AFs to be 0.008 ± 0.002 for FeMn, 0.015 ± 0.005 for PdMn, 0.022 ± 0.005 for IrMn, and 0.060 ± 0.010 for PtMn, respectively. The corresponding spin Hall conductivities (σ_{exp}) are also calculated and shown in Table I. These estimated values are in agreement with the previous analysis using the ratio
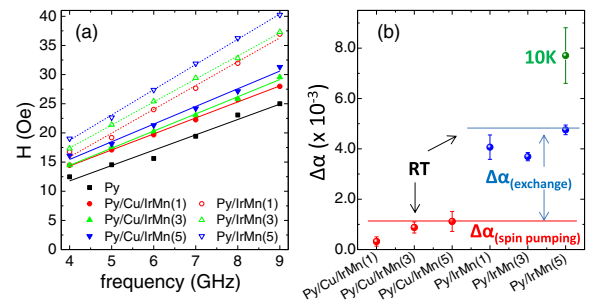

FIG. 4 (color online). (a) Frequency dependence of the linewidth broadening for the IrMn set of samples, and (b) the extraction of the damping enhancement with respect to pure Py at RT and 10 K.

TABLE I. Calculated SHE conductivities σ_{ij}^s for staggered magnetization along a-axis and c-axis directions and comparison with experimental values (σ_{exp}) [units in ($\hbar/e$ S/cm)]. For staggered magnetization along the c axis, PtMn, IrMn, and PdMn exhibit c4 symmetry around the c axis, which results in $\sigma_{yz}^x = -\sigma_{xz}^x$, $\sigma_{zx}^y = -\sigma_{zy}^y$, and $\sigma_{xy}^z = -\sigma_{yx}^z$. Because of the spontaneous magnetic moments on Fe, this symmetry is absent in FeMn.

		σ_{yz}^x	σ_{zy}^x	σ_{zx}^y	σ_{xz}^y	σ_{xy}^z	σ_{yx}^z	$\bar{\sigma}$	σ_{av}	σ_{exp}
PtMn	c axis	303.9	−219.9	219.9	−303.9	60.3	−60.3	194.7	125.2	182.9
	a axis	30.4	−10.5	52.3	−260.9	92.5	−96.5	90.5		
IrMn	c axis	372.8	−59.7	59.7	−372.8	40.9	−40.9	157.8	41.6	40.8
	a axis	−21.3	−94.6	126.3	−351.6	−325.1	325.1	−16.5		
PdMn	c axis	69.5	−17.0	17.0	−69.5	17.8	−17.8	34.8	3.9	33.6
	a axis	0.0	3.5	7.4	−66.8	−70.8	69.8	−11.6		
FeMn	c axis	51.9	48.4	−47.6	50.9	−100.3	96.5	−48.6	−59.0	23.9
	a axis	−82.6	85.9	−47.8	47.5	−121.6	0.0	−64.2		

between ISHE and AMR. Finally, we note that the spin Hall angle for PtMn is comparable to that of Pt obtained by the same experimental approach [24], which opens up the possibility of using PtMn as spin current detector in a variety of AF-spintronics applications.

The Py/AF bilayers showed additional damping enhancement, which is 3 or 4 times larger than in the Py/Cu/AF samples (Fig. 4). We attribute this additional damping enhancement to the FM/AF exchange coupling at the interface. Since AFs usually have relatively high anisotropy, the transfer of the spin angular momentum from precessing FM(Py) to the AF experiences additional dissipation induced by the rigid AF spin lattices under direct FM/AF exchange coupling. We also measured the frequency dependent linewidth at 10 K for one sample, Py(15)/IrMn(5). The damping enhancement is almost doubled compared to that at room temperature, which is also likely due to the enhanced AF anisotropy at lower temperatures [Fig. 4(b)] [37]. This correlation between the damping enhancement and AF anisotropy could be useful for tuning dynamic properties of AF-spintronics devices via engineering the AF anisotropy.

Finally, we compare the experimental estimates of SHE to the intrinsic SHE calculated for ordered PtMn, IrMn, PdMn, and FeMn alloys. The generalized gradient approximation to density functional theory [38] as implemented in the full-potential linearized augmented-plane-wave code FLEUR [39] was employed in the calculations. We took the lattice parameters measured experimentally for the ordered alloys at room temperature: $a = 4.00$ Å and $c = 3.67$ Å for PtMn, $a = 3.855$ Å and $c = 3.644$ Å for IrMn, $a = 4.07$ Å and $c = 3.58$ Å for PdMn, and $a = c = 3.63$ Å for FeMn. In the ordered alloys, the staggered magnetization is along the c axis in PtMn and along the a axis in PdMn and IrMn [40]. FeMn is a noncollinear antiferromagnet [41]. Since the magnetic structure of the thin layers of $Pt_{50}Mn_{50}$, $Ir_{50}Mn_{50}$, $Pd_{50}Mn_{50}$, and $Fe_{50}Mn_{50}$ on Py is not known, we therefore performed calculations of the electronic structure assuming collinear antiferromagnetic order with a staggered magnetization direction along the a axis as well as

along the c axis and averaged the SHE conductivity with respect to the staggered magnetization direction. Spin-orbit interaction was included in the calculations. The intrinsic spin Hall conductivity is given by

$$\sigma_{ij}^s = \frac{-2e\hbar}{N} \sum_{\mathbf{k}} \sum_{\epsilon_{\mathbf{k}n} < E_F < \epsilon_{\mathbf{k}m}} \mathrm{Im} \frac{\langle \mathbf{k}n | Q_i^s | \mathbf{k}m \rangle \langle \mathbf{k}m | v_j | \mathbf{k}n \rangle}{(\epsilon_{\mathbf{k}n} - \epsilon_{\mathbf{k}m})^2},$$

(3)

where E_F is Fermi energy, N is the number of k points $\mathbf{k}$, $\epsilon_{\mathbf{k}n}$ is the band energy, v_j is the velocity component in direction j, and $Q_i^s = (\hbar/4V)[\sigma_s v_i + v_i \sigma_s]$ is the spin current density operator for spin current flowing in the i direction with spin pointing in the s direction. Here, V is the volume of the unit cell and σ_s a Pauli matrix. We employed the Wannier interpolation technique [42] to make the evaluation of Eq. (3) computationally efficient. We constructed 18 maximally localized Wannier functions per atom describing the valence states [43,44]. A $512 \times 512 \times 512$ Monkhorst-Pack k mesh [45] was employed to perform the Brillouin zone summation in Eq. (3). The resulting SHE conductivities are listed in Table I.

Assuming that the thin layers of $Pt_{50}Mn_{50}$, $Ir_{50}Mn_{50}$, $Pd_{50}Mn_{50}$, and $Fe_{50}Mn_{50}$ on Py are (111) textured and that the individual crystallites are rotated randomly around the (111) direction we obtain polycrystalline average SHE conductivities listed as $\bar{\sigma}$ in Table I for fixed collinear staggered magnetization directions along the a and c directions within the crystallites. Assuming additionally that the direction of the staggered magnetization in the crystallites is random, we compute averaged SHE conductivities as

$$\sigma_{av} = [2\bar{\sigma}(a - \text{axis}) + \bar{\sigma}(c - \text{axis})]/3,$$

(4)

which are also given in the Table I. It is noted that the values for PtMn, PdMn, and IrMn follow qualitatively the trend established by the experiments, which validates the averaging of magnetization directions for polycrystalline films. The larger discrepancy between experiment and theory

observed for FeMn (including a sign difference) may be due to its pronounced noncollinear magnetism.

In summary, we studied four metallic AF materials with the same chemical structure as possible spin current detectors using spin pumping and inverse spin Hall effect. By thickness-dependent measurements, we determined the spin diffusion length of these materials to be all rather short, on the order of 1 nm. We estimated the strength of the spin Hall angle of the four AF materials, in which the PtMn showed a large value, comparable to that of Pt. The estimated spin Hall angles of the four materials follow the relationship PtMn > IrMn > PdMn > FeMn, corroborating the important role of the spin-orbit coupling of the heavy metals for the properties of the Mn-based alloys through orbital hybridization. By comparing samples with and without a Cu spacer, we confirmed an additional damping enhancement due to the exchange coupling at the FM/AF interface, in addition to that induced by the transfer of spin angular momentum from spin pumping. We also performed first-principles calculations of ordered alloys and showed that the value of spin Hall conductivity can vary significantly with crystal orientation and staggered AF magnetization; calculations of averaged spin Hall conductivities for polycrystalline systems are in agreement with our experimental results for PdMn, IrMn, and PtMn. Future works on ordered epitaxial systems may allow tailoring the sign and magnitude of the spin Hall conductivities by manipulating the growth along different crystal orientations in these antiferromagnets.

[1] M. I. D'yakonov and V. I. Perel, Sov. Phys. JETP Lett. **13,** 467 (1971).

[2] J. E. Hirsch, Phys. Rev. Lett. **83,** 1834 (1999).

[3] E. Saitoh, M. Ueda, H. Miyajima, and G. Tatara, Appl. Phys. Lett. **88,** 182509 (2006).

[4] S. D. Bader and S. S. P. Parkin, Annu. Rev. Condens. Matter Phys. **1,** 71 (2010).

[5] A. Hoffmann, IEEE Trans. Magn. **49,** 5172 (2013).

[6] L. Liu, C.-F. Pai, Y. Li, H. W. Tseng, D. C. Ralph, and R. A. Buhrman, Science **336,** 555 (2012).

[7] C. Pai, L. Liu, Y. Li, H. W. Tseng, D. C. Ralph, and R. A. Buhrman, Appl. Phys. Lett. **101,** 122404 (2012).

[8] B. F. Miao, S. Y. Huang, D. Qu, and C. L. Chien, Phys. Rev. Lett. **111,** 066602 (2013).

[9] A. Azevedo, O. Alves Santos, G. A. Fonseca Guerra, R. O. Cunha, R. Rodriguez-Suarez, and S. M. Rezende, Appl. Phys. Lett. **104,** 052402 (2014).

[10] A. S. Nunez, R. A. Duine, P. Haney, and A. H. MacDonald, Phys. Rev. B **73,** 214426 (2006).

[11] A. B. Shick, S. Khmelevskyi, O. N. Mryasov, J. Wunderlich, and T. Jungwirth, Phys. Rev. B **81,** 212409 (2010).

[12] V. M. T. S. Barthem, C. V. Colin, H. Mayaffre, M.-H. Julien, and D. Givord, Nat. Commun. **4,** 2892 (2013).

[13] B. G. Park *et al.*, Nat. Mater. **10,** 347 (2011).

[14] J. B. S. Mendes, R. O. Cunha, O. Alves Santos, P. R. T. Ribeiro, F. L. A. Machado, R. L. Rodriguez-Suarez, A. Azevedo, and S. M. Rezende, Phys. Rev. B **89,** 140406(R) (2014).

[15] R. Shindou and N. Nagaosa, Phys. Rev. Lett. **87,** 116801 (2001).

[16] H. Chen, Q. Niu, and A. H. MacDonald, Phys. Rev. Lett. **112,** 017205 (2014).

[17] F. Freimuth, S. Blügel, and Y. Mokrousov, Phys. Rev. Lett. **105,** 246602 (2010).

[18] P. Merodio, A. Ghosh, C. Lemonias, E. Gautier, U. Ebels, M. Chshiev, H. Bea, V. Baltz, and W. E. Bailey, Appl. Phys. Lett. **104,** 032406 (2014).

[19] A. Ghosh, S. Auffret, U. Ebels, and W. E. Bailey, Phys. Rev. Lett. **109,** 127202 (2012).

[20] H. Kurt, R. Loloee, K. Eid, W. P. Pratt, Jr., and J. Bass, Appl. Phys. Lett. **81,** 4787 (2002).

[21] J.-C. Rojas-Sanchez, N. Reyren, P. Laczkowski, W. Savero, J. P. Attane, C. Deranlot, M. Jamet, J.-M. George, L. Vila, and H. Jaffres, Phys. Rev. Lett. **112,** 106602 (2014).

[22] R. Acharyya, H. Y. T. Nguyen, W. P. Pratt, Jr., and J. Bass, IEEE Trans. Magn. **46,** 1454 (2010).

[23] R. Acharyya, H. Y. T. Nguyen, W. P. Pratt, Jr., and J. Bass, J. Appl. Phys. **109,** 07C503 (2011).

[24] W. Zhang, V. Vlaminck, J. E. Pearson, R. Divan, S. D. Bader, and A. Hoffmann, Appl. Phys. Lett. **103,** 242414 (2013).

[25] O. Mosendz, J. E. Pearson, F. Y. Fradin, G. E. W. Bauer, S. D. Bader, and A. Hoffmann, Phys. Rev. Lett. **104,** 046601 (2010).

[26] O. Mosendz, V. Vlaminck, J. E. Pearson, F. Y. Fradin, G. E. W. Bauer, S. D. Bader, and A. Hoffmann, Phys. Rev. B **82,** 214403 (2010).

[27] V. Vlaminck, J. E. Pearson, S. D. Bader, and A. Hoffmann, Phys. Rev. B **88,** 064414 (2013).

[28] A. Scholl, M. Liberati, E. Arenholz, H. Ohldag, and J. Stohr, Phys. Rev. Lett. **92,** 247201 (2004).

[29] S. Brück, G. Schütz, E. Goering, X. Ji, and K. M. Krishnan, Phys. Rev. Lett. **101,** 126402 (2008).

[30] D. R. Penn and M. D. Stiles, Phys. Rev. B **72,** 212410 (2005).

[31] R. Zhang and R. F. Willis, Phys. Rev. Lett. **86,** 2665 (2001).

[32] T. Ambrose and C. L. Chien, Phys. Rev. Lett. **76,** 1743 (1996).

[33] J. van Driel, F. R. de Boer, K.-M. H. Lenssen, and R. Coehoorn, J. Appl. Phys. **88,** 975 (2000).

[34] K. M. Seemann *et al.*, Phys. Rev. Lett. **104,** 076402 (2010).

[35] H. L. Wang, C. H. Du, Y. Pu, R. Adur, P. C. Hammel, and F. Y. Yang, Phys. Rev. Lett. **112,** 197201 (2014).

[36] Y. Sun *et al.*, Phys. Rev. Lett. **111,** 106601 (2013).

[37] W. Zhang and K. M. Krishnan, Phys. Rev. B **88,** 024428 (2013).

[38] J. P. Perdew, K. Burke, and M. Ernzerhof, Phys. Rev. Lett. **77,** 3865 (1996).

[39] See http://www.flapw.de.

[40] R. Y. Umetsu, A. Sakuma, and K. Fukamichi, Appl. Phys. Lett. **89,** 052504 (2006).

[41] J. Kübler, K.-H. Höck, J. Sticht, and A. R. Williams, J. Phys. F **18,** 469 (1988).

[42] N. Marzari, A. A. Mostofi, J. R. Yates, I. Souza, and D. Vanderbilt, Rev. Mod. Phys. **84,** 1419 (2012).

[43] A. A. Mostofi, J. R. Yates, Y.-S. Lee, I. Souza, D. Vanderbilt, and N. Marzari, Comput. Phys. Commun. **178,** 685 (2008).

[44] F. Freimuth, Y. Mokrousov, D. Wortmann, S. Heinze, and S. Blügel, Phys. Rev. B **78,** 035120 (2008).

[45] H. J. Monkhorst and J. D. Pack, Phys. Rev. B **13,** 5188 (1976).